On the Relationship Between Joint Angular Velocity and Motor Cortical Discharge During Reaching

G. ANTHONY REINA, DANIEL W. MORAN, AND ANDREW B. SCHWARTZ
The Neurosciences Institute, San Diego, California 92121

Received 15 August 2000; accepted in final form 5 February 2001

Reina, G. Anthony, Daniel W. Moran, and Andrew B. Schwartz. On the relationship between joint angular velocity and motor cortical discharge during reaching. *J Neurophysiol* 85: 2576–2589, 2001. Single-unit activity in area M1 was recorded in awake, behaving monkeys during a three-dimensional (3D) reaching task performed in a virtual reality environment. This study compares motor cortical discharge rate to both the hand's velocity and the arm's joint angular velocities. Hand velocity is considered a parameter of extrinsic space because it is measured in the Cartesian coordinate system of the monkey's workspace. Joint angular velocity is considered a parameter of intrinsic space because it is measured relative to adjacent arm/body segments. In the initial analysis, velocity was measured as the difference in hand position or joint posture between the beginning and ending of the reach. Cortical discharge rate was taken as the mean activity between these two times. This discharge rate was compared through a regression analysis to either an extrinsic-coordinate model based on the three components of hand velocity or to an intrinsic-coordinate model based on seven joint angular velocities. The model showed that velocities about four degrees-of-freedom (elbow flexion/extension, shoulder flexion/extension, shoulder internal/external rotation, and shoulder adduction/abduction) were those best represented in the sampled population of recorded activity. Patterns of activity recorded across the cortical population at each point in time throughout the task were used in a second analysis to predict the temporal profiles of joint angular velocity and hand velocity. The population of cortical units from area M1 matched the hand velocity and three of the four major joint angular velocities. However, shoulder adduction/abduction could not be predicted even though individual cells showed good correlation to movement on this axis. This was also the only major degree-of-freedom not well correlated to hand velocity, suggesting that the other apparent relations between joint angular velocity and neuronal activity may be due to intrinsic-extrinsic correlations inherent in reaching movements.

INTRODUCTION

Movement coordinate transformations

The sensorimotor planning of a reaching movement is commonly described by two successive transformations (Flanders et al. 1992): a target in extrinsic space (i.e., visual) is transformed by an extrinsic-to-intrinsic coordinate frame (joint angles, muscle lengths) followed by a kinematic-to-dynamic coordinate frame (joint torques, muscle forces). Our previous work in two dimensions has shown that cortical unit populations in primary motor cortex (M1) encode the hand's velocity in extrinsic parameters (Moran and Schwartz 1999a). In this paper, we compare the relation between cortical activity in M1 and both the extrinsic (hand velocity) and intrinsic (joint angular velocity) parameters of the arm during natural reaching in three dimensions.

Neurophysiological experiments

Beginning with Jackson (1889), locationist concepts have evolved from somatotopic cortical maps to single structure/single coordinate frame hierarchies (Kalaska and Crammond 1992). In such a scheme the motor cortex is generally considered as the cortical output of motor signals, operating as the gateway to the "final common pathway" for muscles (Asanuma and Rosen 1972; Evarts 1968). As such, activity in M1 should be correlated with intrinsic and/or dynamic coordinates, rather than more abstract reference frames, such as extrinsic space. Following a series of experiments with single-joint, single degree-of-freedom (DOF) movements (Evarts 1968; Humphrey et al. 1970; Schmidt et al. 1975), Murphy and colleagues (1982) attempted to correlate joint angular position (intrinsic coordinates) with neural activity in a multi-jointed, reaching task. They found that *1*) there was no simple relationship between the neural activity and the electromyogram (EMG); *2*) neuronal activity related to the shoulder joint was similar to neuronal activity related to the elbow joints even though motion about those joints could be quite different; and *3*) the discharge of the shoulder-related neurons seemed to vary systematically with the trajectory.

More recent experiments have shown that several cortical motor areas project to the spinal motor centers (Martino and Strick 1987), and paradigms using natural arm movements (Georgopoulos et al. 1982; Schwartz et al. 1988) have concluded that motor cortical activity is related well to the direction of the hand in space (extrinsic coordinates). Other experiments show that motor cortical activity can even be related to nonmotor aspects of the task (Carpenter et al. 1999; Georgopoulos et al. 1989, 1992). The specific function of the primary motor cortex is still controversial and has been the goal of several studies that have attempted to categorize motor cortical activity to a specific place in the hierarchical set of transformations from vision to muscle activation (Evarts 1968; Humphrey 1986; Kakei et al. 1999; Kalaska and Crammond 1992).

Address for reprint requests: A. B. Schwartz, The Neurosciences Institute, 10640 John Jay Hopkins Dr., San Diego, CA 92121 (E-mail: aschwartz@nsi.edu).

The costs of publication of this article were defrayed in part by the payment of page charges. The article must therefore be hereby marked "*advertisement*" in accordance with 18 U.S.C. Section 1734 solely to indicate this fact.

The question of whether motor cortical activity is representative of intrinsic or extrinsic coordinates is one aspect of this hierarchical scheme. While the work of Georgopoulos and colleagues (Georgopoulos et al. 1982; Schwartz et al. 1988) showed that motor cortical activity was correlated well to extrinsic coordinates, it was not clear whether the task (center→out reaching) could clearly dissociate the two coordinate frames. An attempt to make this distinction by having the animal perform the task in spatially separated regions of the workspace (Caminiti et al. 1990) showed that, although there was a global tendency across the population of recorded units for an orderly shift in preferred directions, this was difficult to see in individual units as shoulder azimuth varied across different regions of space. Interestingly, the statistical shift in preferred direction did not affect the population vector direction. Another experiment (Scott and Kalaska 1995, 1997) compared responses of motor cortical cells as the arm was held in two different postures. Although it was concluded that arm configuration caused a change in preferred direction, only about one-half of the cells had a statistically significant change in their preferred direction between the two postures. Less than 30% of units in this study had preferred directions separated by more than (±45°), and these differences were insufficient to cause a directional shift in the calculated population vectors. A recent study by Kakei and colleagues (1999) used a behavioral paradigm consisting of a single joint (wrist) movement in either a pronated, supinated, or neutral starting position. The different starting positions allowed them to separate three reference frames: based on global hand movement, muscle line-of-action and joint rotation. They found a population (~30%) of cortical units in M1 that were correlated with a muscle coordinate frame (intrinsic) and an even larger population (~50%) that were correlated with the direction of hand movement (extrinsic). They concluded that M1 is involved in "not just the final computation" (i.e., computation of patterns of muscle activity) of the sensorimotor transformation, but in multiple stages of that transformation. These studies are inconsistent with the concept that the motor cortex is isolated on one rung of a hierarchical ladder between intrinsic and extrinsic coordinate systems.

Joint angular velocity population vectors

Population vectors calculated over short intervals predict the movement's kinematics (Moran and Schwartz 1999b; Schwartz 1993; Schwartz and Moran 1999). Although population vectors were originally based on vectorial contributions of neurons in extrinsic two-dimensional (2D) space, they can also be applied to any *n*-dimensional feature space. In this paper we define seven joint angles (i.e., DOF) to describe the arm's configuration: three at the shoulder, one at the elbow, one in the forearm, and two at the wrist. The position of the hand does not uniquely define the arm's configuration; that is, the arm could have many configurations for the same hand location. This is commonly referred to as the "degrees of freedom" problem (Bernstein 1967). Although the DOF problem predicts an infinite number of possible trajectories, reaching movements are quite stereotypical in the relation between intrinsic and extrinsic parameters (Georgopoulos et al. 1981; Helms-Tillery et al. 1995; Soechting and Lacquanti 1981). Soechting and Flanders (1989), for example, found simple linear relationships for arm elevation and yaw angles to target location when humans pointed in the dark. Moran and Schwartz (1999b) found that, in drawing tasks performed by monkeys, there was a very high correlation between individual joint angular velocity and the cosine of hand direction. This suggests that M1 cortical activity, which is highly cosine-tuned to hand velocity in reaching tasks, would also be well correlated to joint angular velocity. In this study, we compared the relationship between hand velocity and cortical discharge to joint angular velocity and cortical discharge.

METHODS

Virtual reality simulator

Two rhesus monkeys (*Macaca mulatta,* 4–6 kg) were operantly trained to perform a 3D center→out reaching task in a virtual reality simulator (Fig. 1). The monkey sat in a primate chair with its head restrained. A custom-made stereo monitor was mounted in front of and above the monkey's head with the screen's display directed downward. A mirror, mounted below the monitor and angled at 45° in the sagittal plane, reflected the display. The monkey viewed the reflected display through a pair of stereographic goggles (CrystalEyes, StereoGraphics). Different viewpoints (parallax values adjusted for inter-ocular distance) of the same image were presented to each eye through these goggles in an alternating, shuttered pattern (120 fields/s) to produce an illusion of depth.

An infrared marker was placed on the dorsum of the monkey's hand. The 3D position of the marker was measured in real-time by an optoelectronic tracking system (Optotrak 3010, Northern Digital). Four other infrared markers recorded positions on the wrist (2), elbow (1), and shoulder (1). A graphics mini-computer (Power Series 4D320VGX, Silicon Graphics) recorded the current position of the monkey's hand and rendered a virtual representation of it to the stereo display. Whenever the monkey moved its hand, it could see a sphere

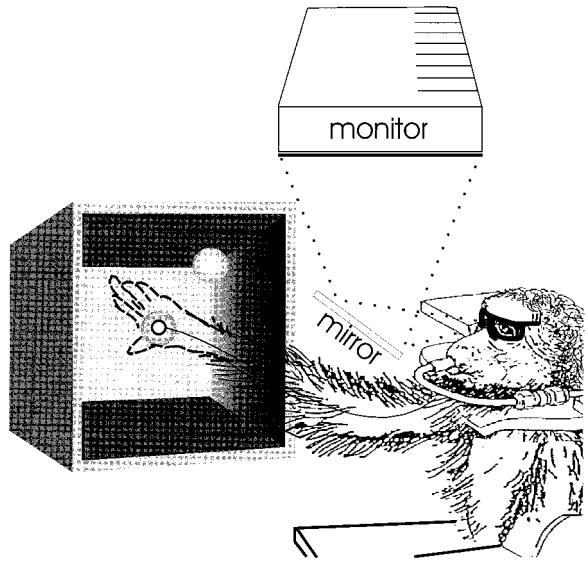

FIG. 1. Illustration of the experimental setup. An opto-electronic tracking device calculated the 3-dimensional (3D) position of the monkey's hand in real-time. A graphics minicomputer used the real-time position data to update an interactive stereoscopic scene projected from a monitor located above and in front of the monkey. A front-silvered mirror reflected the display (dotted lines) through a pair of stereoscopic goggles worn by the monkey. In the virtual scene, a computer-generated sphere floated where the monkey's hand would appear were it able to see its actual hand. As the monkey moved its hand, the cursor sphere moved with the same speed and direction. The virtual workspace for the reach was a cube with a 70-mm face.

(cursor) in the virtual environment move with the same direction and speed. When in the simulator, the monkey could not see its hand or arm; only the virtual representation of hand location. The monkeys received liquid rewards for performing the task correctly. In all cases, the monkeys were treated in accordance with the Institutional Animal Care and Usage Committee and Society for Neuroscience guidelines.

Center→out task

The task began when the monkey touched the cursor sphere to another sphere (center sphere) positioned in the center of the virtual scene. After a random minimum hold time (300–500 ms), the center sphere disappeared and a target sphere appeared at one of eight positions at the corners of a virtual cube centered around the center position (Fig. 1). Each edge of the cube was 70 mm in length, which made the overall movement from the center to the target approximately 60 mm. Once the target sphere appeared, the monkey had a limited time (300–500 ms) to move its hand to the target. After reaching the target sphere and holding that position for a random period (170–500 ms), a reward was given. A new trial began after an inter-trial interval (500–1,000 ms). A reach was performed to each of the eight targets at least five times (minimum 40 total trials) in a random block design.

Cortical recording

The electrophysiological methods and surgical procedures have been described previously in detail (Schwartz 1992). After the monkey had been trained for several months in the center→out task, a circular recording chamber (19 mm diam) was placed over the contralateral motor cortex under general anesthesia of isoflurane, ketamine, and xylazine. The recording chamber was held in place with dental acrylic. On each recording day, the head was immobilized mechanically. A Chubbuck microdrive was mounted on the chamber and hydraulically sealed (Mountcastle et al. 1975). Extracellular recordings were made using glass-insulated, platinum iridium electrodes (1–3 MΩ impedance) attached to the microdrive. The microdrive could position the electrode anywhere within the chamber and its depth within the brain was controlled with 1 μm accuracy. Typically, only one penetration was made each day. Action potentials of single units were identified by the criteria of Mountcastle et al. (1969) and separated using a differential amplitude discriminator. Every attempt was made to record from all cortical layers. For each isolated unit, a center→out task was performed by the monkey followed by a passive examination of the arm to determine whether its activity was related to the movement of a particular body part or joint. Recording sessions ranged from 4–6 h. The monkey was returned to its home cage after each session. Recordings from each hemisphere were performed over a 6- to 8-wk period. Postmortem analysis confirmed that all cortical units analyzed in this study were located rostral to the central sulcus at about the level of the precentral dimple.

Kinematic recording and modeling

In addition to recording the position of the hand, the positions of four other points on the arm were recorded by the optoelectronic recording system. Infrared markers (IRED) were placed on the radial and ulnar sides of the wrist, on the lateral malleolus of the elbow, and just distal to the head of the humerus. The marker data were smoothed using a 10-Hz, low-pass, fifth-order, phase-symmetric digital filter (Woltring 1986). Movement onset and offset times were calculated so that movement onset coincided with the hand speed rising to 25% of maximum and movement offset coincided with the hand speed falling to 35% of maximum. The data were divided into 100 bins. Bin size was calculated by dividing the total movement epoch into 40 equal intervals. Thirty additional bins were assigned just prior to (prebins) and just after (postbins) the movement period and had the same binwidths as the 40 movement bins.

The five IRED markers were used to calculate instantaneous attitude matrices for the humerus, ulna, radius, and hand. The scapula was defined as the inertial reference frame for the kinematic model and was assumed a fixed, global reference frame throughout the movement. The five segmental attitude matrices were used to calculate four rotation matrices corresponding to the modeled joints of the arm (shoulder, elbow, forearm, and wrist). Seven Cardanic angles (Euler permutation x, y', z'') were calculated from the joint rotation matrices and are as follows: shoulder adduction/abduction, shoulder internal/external rotation, shoulder flexion/extension, elbow flexion/extension, radial pronation/supination, wrist flexion/extension, and wrist abduction/adduction.

A forward kinematic arm model was constructed to predict hand position from measured joint angles. Accurate postmortem measurements (segment lengths, joint center locations, etc.) were taken from the dissected arm bones of each subject. These values were averaged across subjects for use in a general monkey arm model. The accuracy of the model was judged by applying a set of averaged joint angle trajectories (across all subjects) to the model and comparing the resulting predicted hand trajectories to the measured hand trajectories (averaged across all subjects). A set of equations for the Jacobian matrix, which relates the partial derivatives of hand coordinates to joint coordinates, were similarly derived from the model. The Jacobian matrix is a function of joint posture; therefore the subjects' average posture during the central hold position was used to define a static Jacobian matrix used in all subsequent analyses. Since there are seven joint angles and only three hand coordinates, the Jacobian is not square (i.e., 3×7). To solve for the inverse kinematic model, a right pseudoinverse of the Jacobian was used as follows

$$\dot{\theta} = J^T(JJ^T)^{-1}\dot{p} \tag{1}$$

where $\dot{\theta} = 7 \times 1$ vector of joint angular velocity, $J = 3 \times 7$ static Jacobian matrix, and $\dot{p} = 3 \times 1$ vector of hand velocity.

Spike rate processing

Only trials that contained a complete set of neural and kinematic data were analyzed. The data consisted of at least 40 trials per cortical unit (5 repetitions each to 8 targets), but in some cases consisted of as many as 160 trials per unit (20 repetitions each to 8 targets). The time epoch analyzed began when the target sphere first appeared and ended when the monkey had moved the cursor sphere to the target sphere and held it within the target sphere for a random period of time (170–500 ms). A partial binning technique was used to determine the discharge rate during the entire time epoch (Richmond et al. 1987; Schwartz 1992).

The square root transformation was performed on the discharge rate to apply standard statistical techniques to the data. Although data transformations are a conservative, statistical necessity to performing parametric tests on data from nonnormal distributions, such as neural discharge rates, we performed the analysis on both the raw and the transformed data to show that the interpretation of the analysis is unaltered by the square root transformation.

Multiple linear regression

HAND VELOCITY TUNING. A multiple linear regression between cortical activity and 3D hand velocity was performed for each cortical unit. The form of the regression equation is

$$\bar{D}_i^* = b_{i,0} + b_{i,x}\bar{\dot{x}} + b_{i,y}\bar{\dot{y}} + b_{i,z}\bar{\dot{z}} \tag{2}$$

where D^* = transformed discharge rate, b_0–b_z = regression coefficients, x = anterior/posterior hand position, y = superior/inferior hand position, z = right/left hand position, and i = cortical unit i.

Also, the bars over the variables represent averages taken over the time bins corresponding to reaction and movement time, and the dots over the variables represent the first derivative with respect to time.

Each movement repetition was an independent observation in the regression. The relationship between the discharge rate and the direction of movement can be described as cosine tuned (Georgopoulos et al. 1982). In *Eq. 2*, this cosine-tuned relationship has been modified to include hand speed (Moran and Schwartz 1999a). The regression coefficients b_x, b_y, and b_z represent the preferred direction vector of a motor cortical unit. The right-hand side of *Eq. 2* (excluding the b_0 term) is a dot product between the preferred direction vector of the cortical unit and hand velocity vector; this is comparable with the cosine of the angle between these two vectors.

JOINT ANGULAR VELOCITY TUNING. The average joint angular velocities of the arm were also used to predict the discharge rate of each cortical unit. Average joint angular velocity was defined as the difference between a joint angle at the beginning and end of the trajectory divided by the movement time. Using a multiple linear regression, cortical activity and joint angular velocity were related by the equation

$$\bar{D}_i^* = b_{i,0} + b_1\bar{\dot{\theta}}_1 + b_{i,2}\bar{\dot{\theta}}_2 + b_{i,3}\bar{\dot{\theta}}_3 + b_{i,4}\bar{\dot{\theta}}_4 + b_{i,5}\bar{\dot{\theta}}_5 + b_{i,6}\bar{\dot{\theta}}_6 + b_{i,7}\bar{\dot{\theta}}_7 \qquad (3)$$

where θ_1 = shoulder adduction/abduction, θ_2 = shoulder internal/external rotation, θ_3 = shoulder flexion/extension, θ_4 = elbow flexion/extension, θ_5 = radial pronation/supination, θ_6 = wrist flexion/extension, and θ_7 = wrist abduction/adduction. The rest of the variables and symbols are defined in *Eq. 2*.

Equation 3 takes the same form as *Eq. 2* except that the *x*, *y*, and *z* cartesian coordinates are replaced by seven cardanic joint coordinates. The regression coefficients in *Eq. 3* (except for b_0) essentially represent a "preferred angular velocity" much like the regression coefficients in *Eq. 2* represent a preferred direction vector. Although the preferred angular velocity vector is seven-dimensional, it can be used in a population vector analysis in a similar manner to 2D and 3D preferred directions.

REGRESSION OPTIMIZATION. The joint angular velocity tuning described above included seven joint angles as independent factors in the regression model. To determine whether all seven joint angular velocities were needed in the model, the relative contribution that each joint angle added to the prediction of the discharge rate was compared. First, the coefficients for each regression were standardized (standard, partial regression coefficients) (Sokal and Rohlf 1997). This allowed comparisons of the relative strengths of the effects of several independent variables on the same dependent variable. The joint angular velocities with larger standard, partial regression coefficients had greater contributions to the fit of the regression model (Ashe and Georgopoulos 1994). Second, the number of factors needed in the regression model was optimized for each of the cortical units. Each average joint angular velocity was considered an independent factor in the model. The computer algorithm called RBEST in the IMSL software package (Visual Numerics, Houston, TX) was used to determine which combination of factors produced the best-fitted regression equation for each task-related unit. The algorithm is based on an efficient technique of considering all possible regression permutations (Furnival and Wilson 1974). A measure of the usefulness of a regression model is the coefficient of determination (r^2), which describes how much of the total variation in the discharge rate can be explained by the regression model. The RBEST algorithm used in this study calculated the adjusted-r^2, which is a normalization of the r^2 that allows a comparison of regression models with different numbers of regressors. The algorithm was used to determine the number and combination of regressors that produced the largest adjusted-r^2. The regression with the largest adjusted-r^2 was termed the "best" regression for that cortical unit.

Population analysis

Two sets of population vectors were calculated as a time series throughout the task: one based on hand velocity tuning and the other on the joint angular velocity tuning. Only units with significant regression equations ($P < 0.01$) recorded from the right hemisphere during reaching with the left arm were used to create population vectors. Population vectors based on the joint angular velocity tuning were calculated using the seven-DOF model.

The population vector is a useful tool for evaluating the collective, predictive power of the cortical units over time. The regression equations described previously were calculated over a single epoch spanning the entire reaction and movement time, making it impossible to use this analysis by itself to describe the temporal variation between movement parameters (i.e., hand velocity or joint angular velocity) and discharge rate. However, the regression result (preferred direction) can be used to calculate population vectors at different times in the task. A time series of population vectors based on instantaneous discharge rate in 9-ms bins was used to compare population activity to movement parameters as they varied throughout the reach (*Eq. 4*).

$$PV_{j,t} = \frac{1}{N}\sum_{i=1}^{N}\left(\frac{D_{i,t}^* - \hat{D}_i^*}{D_{i_{\max}}^* - \hat{D}_i^*}\cdot\frac{b_{i,j}}{\sqrt{\sum_{j=1}^{M} b_{i,j}^2}}\right) \qquad (4)$$

where $PV_{j,t}$ = population vector for coordinate j at time bin t, $D_{i,t}^*$ = transformed discharge rate of cortical unit i at time t, $\hat{D}_i^*$ = geometric mean of transformed discharge rate of unit i over all movements, $D_{i_{\max}}^*$ = maximum transformed discharge rate of unit i over all movements, $b_{i,j}$ = regression coefficient for cortical unit i and coordinate j, N = number of cortical units, and M = number of regression factors (hand velocity = 3, joint angular velocity = 7).

The results of *Eq. 4* were integrated in time to yield a population trajectory. In the case of hand velocity tuning information, the population trajectory was directly compared with the actual hand path during the movement. When integrating the joint angle population vectors, the initial posture of the arm (i.e., joint angles during initial position at the center target) was used as the integration constant. The resulting joint angle population trajectories were then applied to a forward kinematic model of the arm to yield a predictive hand trajectory. Because the population vectors were created using the discharge rates of cortical units that precede the actual movement of the arm, a time lag was incorporated in the discharge rate of the unit. This lag was iteratively increased from zero until the root-mean-squared (RMS) error between the population trajectories and the actual hand trajectory was minimized.

RESULTS

A total of 298 cortical units from 3 hemispheres of 2 monkeys were individually recorded during the center→out task (n = 18,272 reaches; average of 7.7 reaches per target per cortical unit). These units were all located in the proximal-arm area of the primary motor cortex (Fig. 2). The frequency of discharge in 227 of the 298 units (76.1%) varied with the target direction (ANOVA, $P < 0.05$). Only these 227 "task-related" units were furthered analyzed (n = 13,976 reaches).

Kinematics

The mean speed profiles (n = 13,976) for each coordinate of the hand velocity and joint angular velocity for all movements are shown in Fig. 3. Average reaction and movement times were 281.0 ± 71.8 (SD) ms and 374.6 ± 95.8 ms, respectively. The hand speeds (Fig. 3*A*) followed a bell-shaped curve in all three dimensions, and their relative timings suggest that the

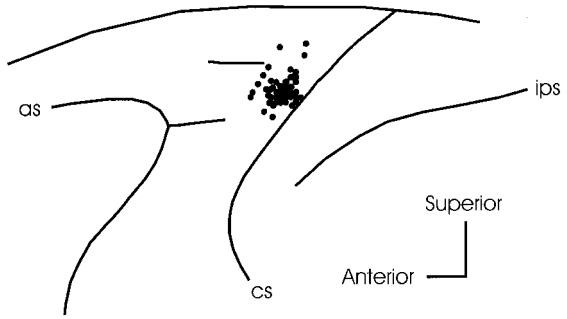

FIG. 2. Electrode penetrations. Only penetrations anterior to the central sulcus were analyzed. cs, central sulcus; as, arcuate sulcus; ips, intraparietal sulcus.

reaching movement was made initially in the frontal plane because the superior/inferior and the right/left speeds peaked around 450 ms while the anterior/posterior speed crested approximately 40 ms later. Shoulder internal/external rotation and adduction/abduction speeds peaked just prior to the frontal plane hand speeds while shoulder and elbow flexion were delayed and corresponded with anterior/posterior hand speeds.

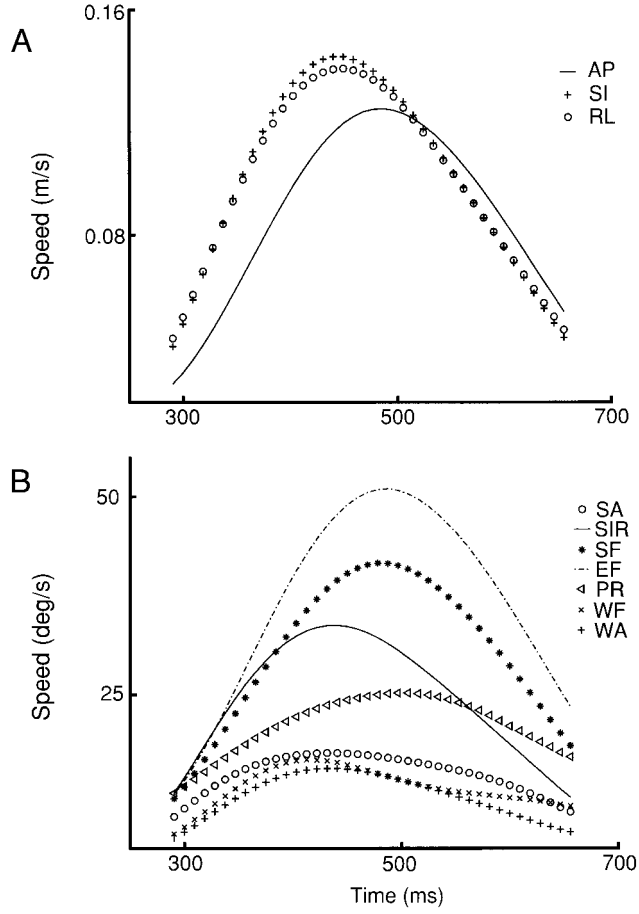

FIG. 3. Individual coordinate speeds. *A*: hand speeds for the anterior/posterior (AP), superior/inferior (SI), and right/left (RL) coordinates. The AP coordinate (depth) peaks later than the 2 frontal-plane coordinates. *B*: joint speeds for shoulder adduction/abduction (SA), shoulder internal/external rotation (SIR), shoulder flexion/extension (SF), elbow flexion/extension (EF), forearm pronation/supination (PR), wrist flexion/extension (WF), and wrist adduction/abduction (WA). Shoulder and elbow flexion tend to peak later than the other joint coordinates, which suggests that their dominate effect is on AP depth.

TABLE 1. *Correlation coefficients of the average hand velocities during center→out task*

	Anterior Velocity	Superior Velocity	Right Velocity
Anterior velocity	1.000		
Superior velocity	0.001 ± 0.176	1.000	
Right velocity	−0.048 ± 0.167	−0.016 ± 0.148	1.000

Values are means ± SD. The calculated tolerances for all 3 were greater than 0.99.

Correlations between regression factors

The mean and standard deviation for the Pearson correlation coefficients between the anterior, superior, and right velocities and between all joint angular velocities are shown in Tables 1 and 2. As expected, there were very low correlations and standard deviations between the anterior, superior, and right velocities. The standard deviations for the correlation between joint angular velocities were much larger and indicated that these correlations varied widely from trial to trial. Shoulder flexion velocity and elbow flexion velocity had a large correlation coefficient ($r = -0.672$). The same was true for shoulder adduction and internal rotation ($r = -0.643$). Large correlations suggest co-linearity among the joint angular velocities, which could distort the regression model. A tolerance calculation, which is the reciprocal of the variance-inflation factor (VIF), was performed. A tolerance value of <0.25 typically indicates that the correlation between regression factors is significant and will greatly affect the results of the regression model. The tolerance calculated over all trials was >0.3 (VIF < 3.3). Although the correlations coefficients were large, each joint angular velocity could be considered an independent regressor in the model.

Although the individual components within a reference frame could be considered independent for the regression model, the intrinsic and extrinsic reference frames were well-correlated to each other. This high correlation is demonstrated in Table 3. For each monkey, the three hand velocity components (anterior/posterior, superior/inferior, right/left) were used as independent regression factors to predict the joint angular velocity at any movement time (i.e., at each of the 40 movement bins) within the eight-target workspace (*monkey F*, right arm = 126,080 observations, left arm = 176,640 observations; *monkey G*, left arm = 256,320 observations). As seen in Table 3, the three hand velocity components were able to predict all of the joint angular velocities well (all regressions significant, $P < 0.00001$). Notably, shoulder internal/external rotation, shoulder flexion/extension, and elbow flexion/extension could be predicted almost exactly from the hand velocity components ($r^2 > 0.9$).

Kinematic model of the arm

The seven measured joint angles were applied to a forward-kinematic skeletal model of the arm to yield a prediction of hand trajectory. Figure 4 shows a typical comparison of an actual hand path (—) and the hand path predicted by applying the measured joint angles to the skeletal arm model (○). The mean RMS error is 4.5 mm for the 60-mm task. The skeletal model was able to predict the hand trajectory from the measured joint angles with approximately a 7% error.

TABLE 2. *Correlation coefficients of the average joint angular velocities during the center→out task*

	Shoulder Adduction	Shoulder Internal Rotation	Shoulder Flexion	Elbow Flexion	Pronation	Wrist Flexion	Wrist Abduction
Shoulder adduction	1.000						
Shoulder internal rotation	−0.643 ± 0.213	1.000					
Shoulder flexion	−0.537 ± 0.276	−0.061 ± 0.164	1.000				
Elbow flexion	0.357 ± 0.281	0.085 ± 0.175	−0.672 ± 0.101	1.000			
Pronation	−0.112 ± 0.423	0.290 ± 0.324	−0.196 ± 0.504	0.376 ± 0.580	1.000		
Wrist flexion	−0.432 ± 0.321	0.387 ± 0.323	0.217 ± 0.328	−0.413 ± 0.371	−0.052 ± 0.530	1.000	
Wrist abduction	0.261 ± 0.339	−0.260 ± 0.313	−0.046 ± 0.405	0.362 ± 0.532	−0.202 ± 0.474	−0.536 ± 0.429	1.000

Values are means ± SD. The calculated tolerances for all 7 were greater than 0.3.

The Jacobian matrix assumes that joint angle and endpoint velocities are well related in a given region of the workspace. Predicting joint angular velocities from measured hand velocities using the pseudoinverse of the Jacobian yielded similar results to the correlations between regression factors described above. In Fig. 5, the actual and Jacobian-predicted angular velocities for shoulder flexion/extension and shoulder adduction/abduction are plotted for reaches to two targets (*targets 3* and *6*). Throughout the entire workspace, shoulder flexion, shoulder internal rotation, and elbow flexion velocity were well predicted by the static Jacobian. However, this was not so for shoulder adduction velocity and the distal joint angular velocities. Both the Jacobian and correlation analyses show that hand velocity is correlated to shoulder flexion, shoulder internal rotation, and elbow flexion, with a lack of correlation between hand velocity and the other four joint angular velocities.

Multiple regression analysis

Figure 6*A* shows a histogram of significant adjusted-r^2 values for regressions to hand velocity and joint angular velocity (JAV). A total of 204 (89.9%) of the 227 units had significant regressions to the hand velocity, while 192 units (84.6%) had significant regressions to the joint angular velocities ($P < 0.01$). Significant regressions to both hand and joint angular velocities were found in 186 units (81.9%). The mean adjusted-r^2 for the JAV model ($\mu = 0.363$; $\sigma = 0.218$) was smaller than for the hand velocity model ($\mu = 0.511$; $\sigma = 0.203$). Figure 6*B* shows the cumulative frequency distribution of the *P* values for all regressions. The two plots overlap indicating that both regressions provide equally significant predictions of the cortical discharge rate (Kolmogorov-Smirnov 2-sample test, $P = 0.289$).

TABLE 3. *r^2 for a regression model using the three components of hand velocity (anterior/posterior, superior/inferior, right/left) to predict a joint angular velocity*

	r^2		
Joint Angular Velocity	*monkey F*, arm R	*monkey F*, arm L	*monkey G*, arm L
Shoulder adduction/abduction	0.626	0.526	0.531
Shoulder internal/external rotation	0.955	0.950	0.938
Shoulder flexion/extension	0.957	0.955	0.915
Elbow flexion/extension	0.957	0.968	0.922
Pronation/supination	0.343	0.544	0.045
Wrist flexion/extension	0.192	0.271	0.285
Wrist abduction/adduction	0.209	0.161	0.478

Each of the 40 movement bins to each of the 8 targets for each repetition is considered an observation in the regression [*monkey F*, right arm = 126,080 observations (40 bins × 8 targets × 394 repetitions), left arm = 176,640 observations (40 bins × 8 targets × 552 repetitions); *monkey G*, left arm = 256,320 observations (40 bins × 8 targets × 801 repetitions)]. The results suggest that the extrinsic and intrinsic references frames are well-correlated for the movements within this workspace (all $P < 0.00001$).

The results for a typical unit (*FL128*) using the hand velocity model are shown in Fig. 7. The relationship between the actual and predicted discharge rates (Fig. 7*A*) was linear (adjusted-$r^2 = 0.634$; $P < 0.0001$). The residual error versus predicted discharge rate from the regression (Fig. 7*B*) was representative of 181 of 227 units used (79.7%). No discernable trend exists in the residuals. The cumulative distribution of the residuals (Fig. 7*C*) was fairly linear, indicating that the residual error was normal in its distribution. One limitation of the model was that it could not accurately predict a discharge rate of 0 Hz. The predicted discharge rate could be 0 Hz only when the hand speed was zero throughout the task. This limitation of the model was evident in 46 of the 227 regressions (20.3%). For example, the plot of the actual versus predicted discharge rate for *unit GR26* (Fig. 8*A*) contained data points where the actual discharge rate was 0 Hz, but the predicted discharge rate was nonzero. The residual versus predicted plot (Fig. 8*B*) contained

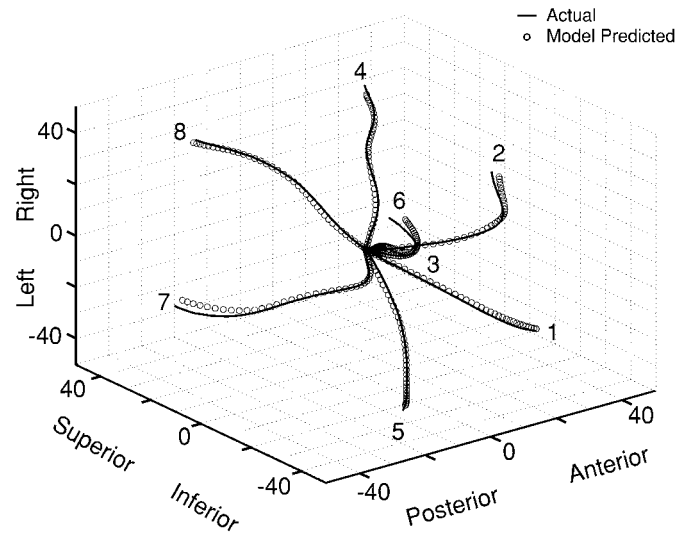

FIG. 4. Comparison of actual hand trajectories and those based on recorded joint angles applied to a forward kinematic model of the arm. The high correlation suggests that accurate joint angles were measured and that 7 degrees-of-freedom (DOF) is sufficient to model a monkey's arm.

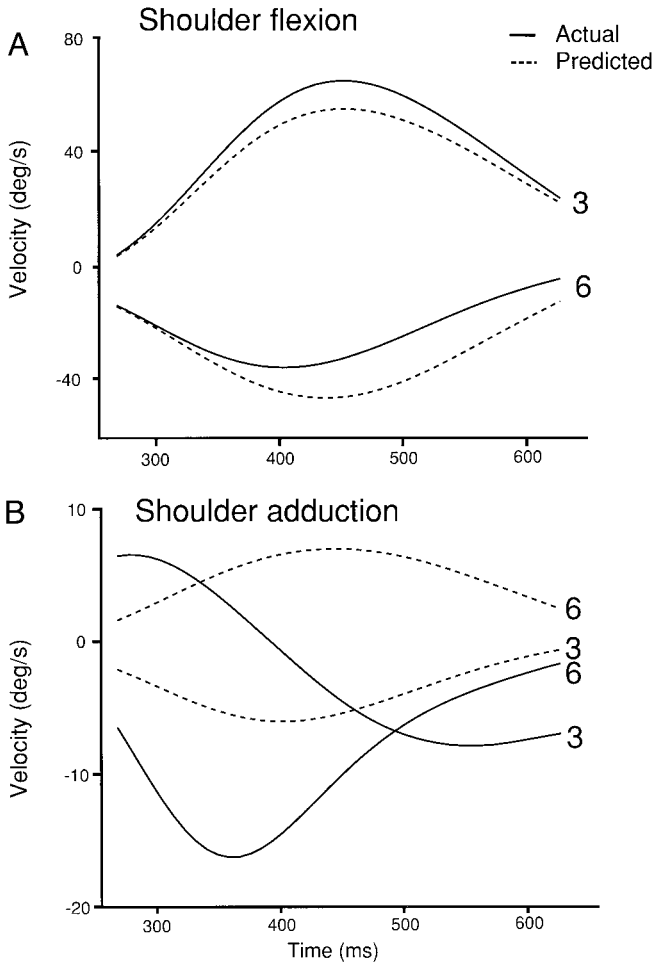

FIG. 5. Joint angular velocities for (*A*) shoulder flexion/extension and (*B*) shoulder adduction/abduction to 2 reaching targets (*3*: superior, left, anterior; *6*: inferior, right, posterior). The solid line is the actual angular velocity, and the dashed line is the angular velocity predicted using the Jacobian matrix that was calculated at the initial arm position. Elbow flexion/extension and shoulder internal/external rotation were as well predicted as shoulder flexion/extension. This complements the finding that a simple, linear regression could be used to predict these three joint angular velocities from the hand velocities. Pronation/supination and the wrist were as poorly predicted as shoulder adduction/abduction.

a linear portion around 0 Hz, reflecting this nonzero prediction of the discharge rate (adjusted-$r^2 = 0.720$; $P < 0.0001$). All of these cases occurred when the discharge rate was <10 Hz. This reflects a limitation of the regression model for units with low discharge rates. The cumulative frequency of the residuals only deviated slightly from linearity as the residual value increased (Fig. 8*C*).

The results for the typical unit (*FL128*) using the JAV model with seven DOF are shown in Fig. 9. As with the hand model, the relationship between the actual and predicted discharge rates (Fig. 9*A*) was linear (adjusted-$r^2 = 0.338$; $P < 0.0001$). This was representative of 179 of the 227 units used (78.9%). No discernable trend exists in the residuals (Fig. 9*B*). The cumulative distribution of the residuals (Fig. 9*C*) indicated that the residual error was normal in its distribution. The JAV model also had the limitation at low discharge rates found in the hand model. This limitation of the model was evident in 48 of the 227 regressions (21.1%).

Optimal regression

Figure 10 shows how often each factor had the largest standard partial regression coefficient. In the hand velocity model, the anterior/posterior velocity (51.5%) most frequently was the factor that explained most of the variance in discharge rate (Fig. 10*A*). The superior/inferior (23.5%) and right/left velocities (25.0%) made similar contributions to the model. In the JAV model, three angles accounted for 76.6% of the variance (Fig. 10*B*). The standard, partial regression coefficients for shoulder flexion, elbow flexion, and shoulder internal rotation were most frequently ranked first in all regression equations. Wrist flexion and pronation contributed the least to the regression. They were ranked first for only 2.1 and 3.1% of the regressions, respectively.

In the regression analyses above, three regression factors were used for the hand velocity model, and seven regression factors were used for the JAV model. Using the RBEST algorithm described in METHODS, we determined whether the full model (i.e., using all regression factors) was necessary to obtain the best-fitted regression. The best regressions for the hand velocity model (Fig. 11*A*) most frequently involved the full model (i.e., all 3 factors). In contrast, the best regressions for the JAV model most frequently involved only a partial model. More than one-half (63.6%) of the best-fitted regressions for the JAV model required four or less factors (Fig.

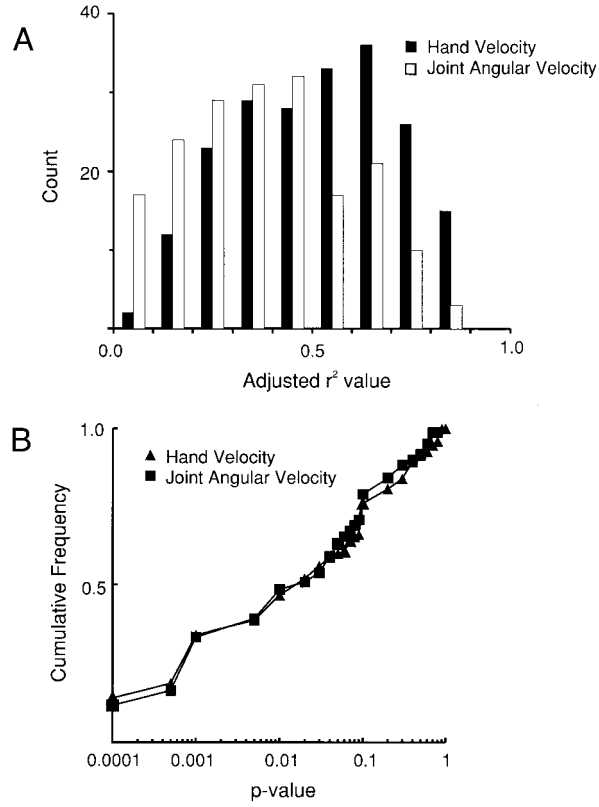

FIG. 6. Results of a multiple regression analysis of arm kinematics on single cortical unit data. *A*: histogram of adjusted-r^2 for both the hand velocity model (*Eq. 2*) and joint angular velocity (JAV) model (*Eq. 3*). The mean adjusted-r^2 for JAV model ($\mu = 0.363$; $n = 192$) is lower than the hand velocity model ($\mu = 0.511$; $n = 204$). *B*: cumulative frequencies of *P*-values for the 2 models. The high degree of overlap in the 2 curves shows that the 2 models were equivalent in explaining the variance of the cortical unit's discharge rate.

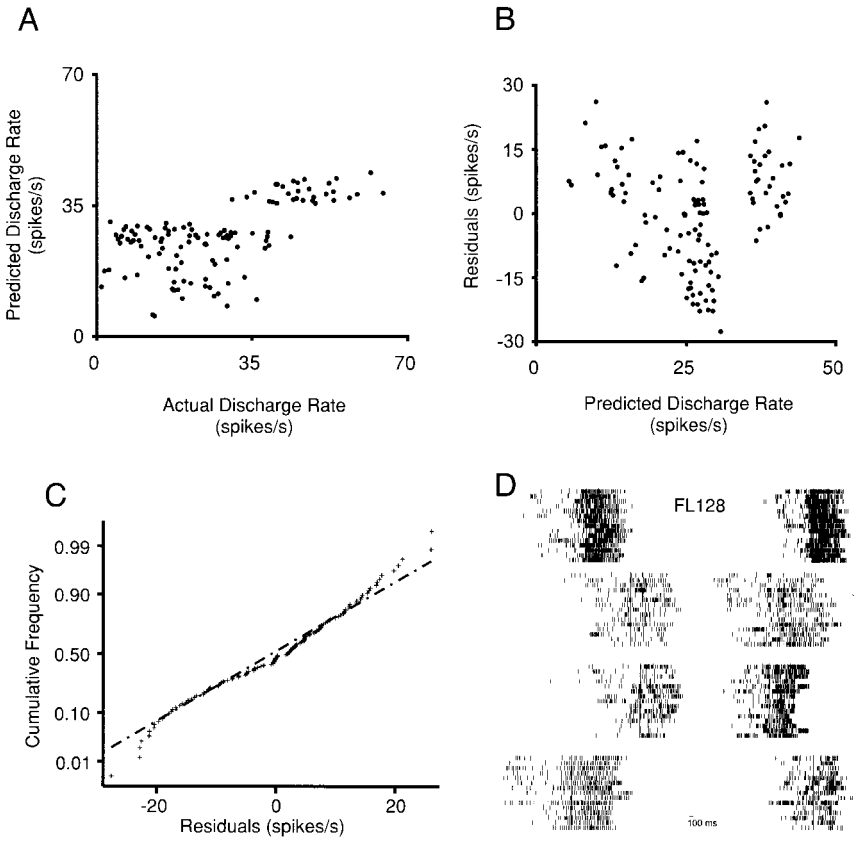

FIG. 7. Regression results for an example cortical unit (*FL128*) using the hand velocity model. *A*: comparison of predicted vs. actual firing rate. *B*: comparison of the residual error vs. the predicted firing rate. Plotting the residuals (predicted − actual discharge rates) against the predicted discharge rate shows that the error is random. *C*: cumulative frequency of residuals. Plotting the residuals on a cumulative-frequency Gaussian scale verified that the residuals were normally distributed (i.e., linear result between 1st and 3rd quartile). *D*: raster plot of the raw discharge times to each target. This type of result was found for 80% of the movement-related cortical units. Anterior targets are plotted closer to the center of the graph (*rows 2* and *3*: counter-clockwise from *bottom left*: *targets 1, 3, 4, 2*). Posterior targets are plotted closer to the edges of the graph (*rows 1* and *4*: counter-clockwise from *bottom left*: *targets 5, 7, 8, 6*). The line at the *bottom* is approximately 100 ms.

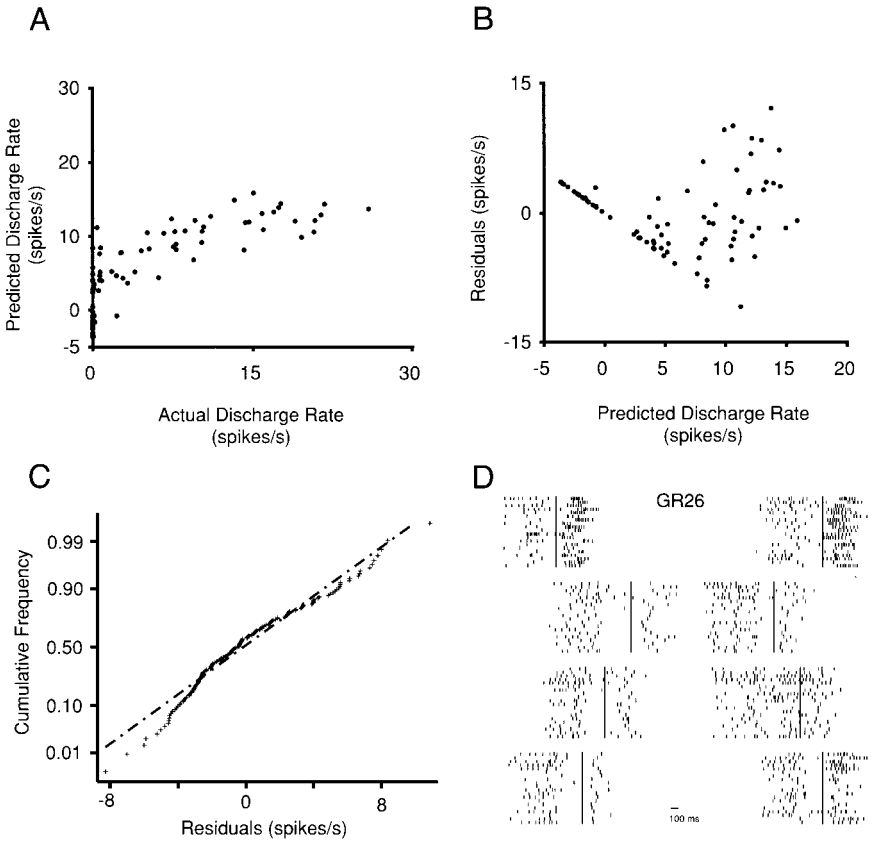

FIG. 8. Regressions results for a low-firing cortical unit (*GR26*) using the hand velocity model. *A*: comparison of predicted vs. actual firing rate. *B*: comparison of the residual error vs. the predicted firing rate. The residuals show a nonrandom error. *C*: cumulative frequency of residuals. Like Fig. 7*C*, the residuals for these low firing units (20% of total) were normally distributed. *D*: raster plot of the raw discharge times to each target. Format is as Fig. 7*D*.

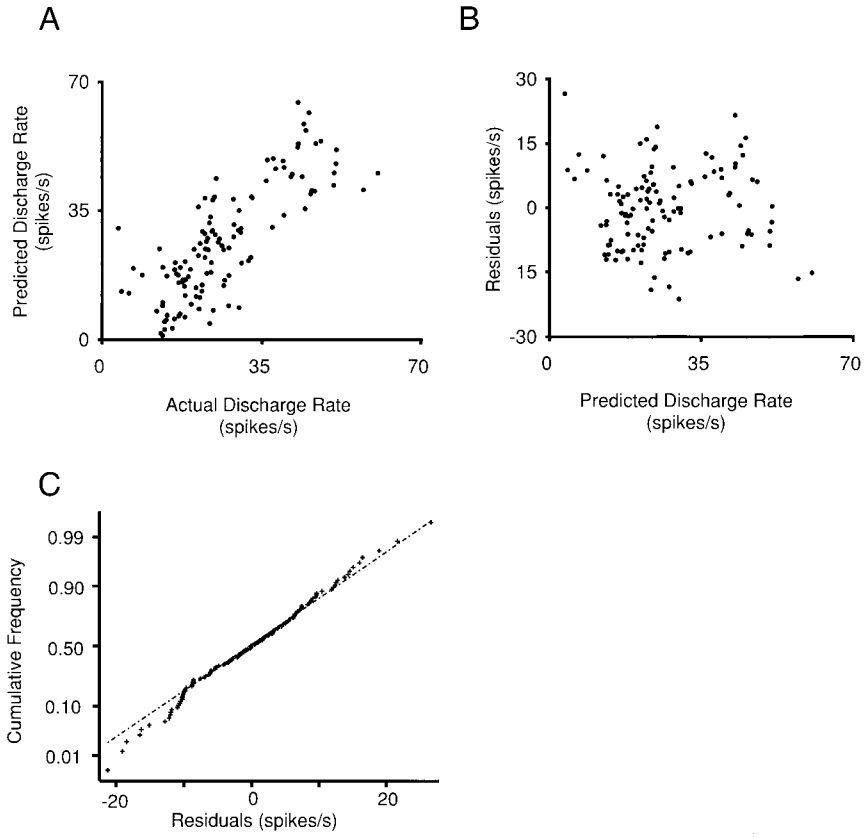

FIG. 9. Regression results for an example cortical unit (*FL128*) using the JAV model with 7 regression coefficients. *A*: comparison of predicted vs. actual firing rate. *B*: comparison of the residual error vs. the predicted firing rate. Similar to Fig. 7*B*, no discernable pattern emerges from the residuals of JAV model. *C*: cumulative frequency of residuals. As in Figs. 7*C* and 8*C*, a linear relationship shows that the residuals were normally distributed.

11*B*). Eighty-nine percent of the regressions required five factors or less in the model. Only 2% of the regressions required the full model (i.e., all 7 regression factors) for the best-fit.

Effects of the square-root transformation

It has been suggested that the square root transformation is a "major statistical bias" that skews this type of statistical analysis (Todorov 2000). A square root transformation is mathematically required when analyzing nonnormal data, such as cortical discharge rates, with parametric statistical tests. Nevertheless, we repeated our analysis using raw discharge rates (single bin, no square root transformation). The number of statistically significant regression equations to hand velocity decreased from 89.9% (204 of 227) for the square-root transformed data to 84.9% (191 of 225) for the raw data. Similarly, the number of statistically significant regressions to joint angular velocities decreased from 84.6% (192 of 227) to 82.7% (186 of 225). The contribution of the regression factors remained essentially the same in both cases as seen in Table 4. The square root transform in no way skewed the interpretation of the results.

Population vector analysis

The three dimensions of hand velocity and the four dominant joint angular velocities were predicted from the cortical discharge rates using the population vector analysis. As described in METHODS, the population vector made with hand velocity tuning used a three-DOF model, and the population vector made with the joint angle tuning used a seven-DOF model. Only units with significant regression equations ($P < 0.01$) recorded from the right hemisphere during reaching with the left arm were used to create population vectors ($n = 156$ cortical units for hand velocity tuning; $n = 145$ cortical units for JAV tuning).

The predicted speed profiles for shoulder adduction/abduction, shoulder internal/external rotation, shoulder flexion/extension, and elbow flexion/extension are plotted in Fig. 12. The plots represent the average speed profiles for each of the eight movements predicted by the population vector model. Although the relative bell shapes of the predicted profiles approximate the actual speed profiles (Fig. 3), there are subtle differences in the relative peaks. Most notably, shoulder and elbow flexion/extension peak almost simultaneously in the actual reach, but shoulder flexion precedes elbow flexion by over 70 ms in the population vector prediction (for comparison, Fig. 3 vs. Fig. 12). In addition, the maximal speed predicted for shoulder adduction is approximately one-half of the actual speed obtained during the reach. The remaining three profiles give a better prediction of the actual peak speed for their respective joint angles.

The predicted velocity profiles for shoulder adduction/abduction and shoulder flexion/extension are plotted in Fig. 13. The plot represents the velocity profile predicted by the population vector model to two of the targets (*3*: superior, left, anterior; *6*: inferior, right, posterior). The predicted velocity profile for shoulder adduction to *target 3* is poor (%RMS error = 267). In general, the percentage of RMS error between the actual and predicted joint angular velocities was lowest for shoulder flexion/extension, elbow flexion/extension, and shoulder internal/external rotation. Further, the velocity profile

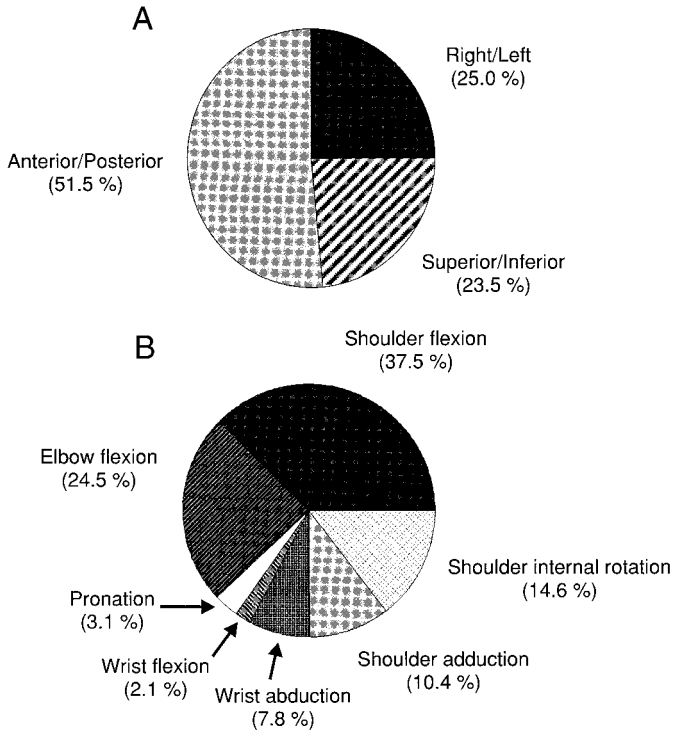

FIG. 10. Percentages of coordinates that had the largest, standard, partial regression coefficient for each cortical unit using both the hand velocity model (*A*) and the JAV model (*B*). Anterior/posterior hand velocity was the dominant coordinate in the hand model, while shoulder and elbow flexion were dominant in the JAV model. Forearm and wrist angular velocities rarely dominated the regression.

predicted from the population vector model did not necessarily agree with that predicted from the Jacobian model. For example, the velocity profiles predicted by the population vector model (Fig. 13) differ from those of the Jacobian model (Fig. 5).

The population vector–derived trajectories of hand (green) and joint angular velocity (blue) are displayed in Fig. 14. Superimposed on this plot is the actual trajectory of the hand during the task (red). The minimum, average RMS errors between actual and predicted trajectories were 3.23 mm for the hand and 5.68 mm for the joint angles. These were found at a lead of 102 ms for the hand velocity model and 121 ms for the joint angular velocity model. Qualitatively there appears to be greater errors in the prediction to some targets using the joint angle tuning than the hand velocity tuning. However, no clear difference between the RMS errors of the two population trajectories can be demonstrated since the kinematic arm model adds, on average, a 4.5-mm error to the JAV-derived hand trajectory.

One bias that can limit the accuracy of a population vector approach is a preferred directional space that is not uniform. In other words, if the regression coefficients for the units were not uniformly distributed, then the population vector may be skewed. For example, if there were a high percentage of preferred directions to the right (in the case of hand velocity), then the population vector could be improperly skewed along that axis.

To test whether the regression coefficients formed a uniform distribution, we performed a bootstrap analysis. In the case of the JAV, the regression coefficients for each unit were consid-

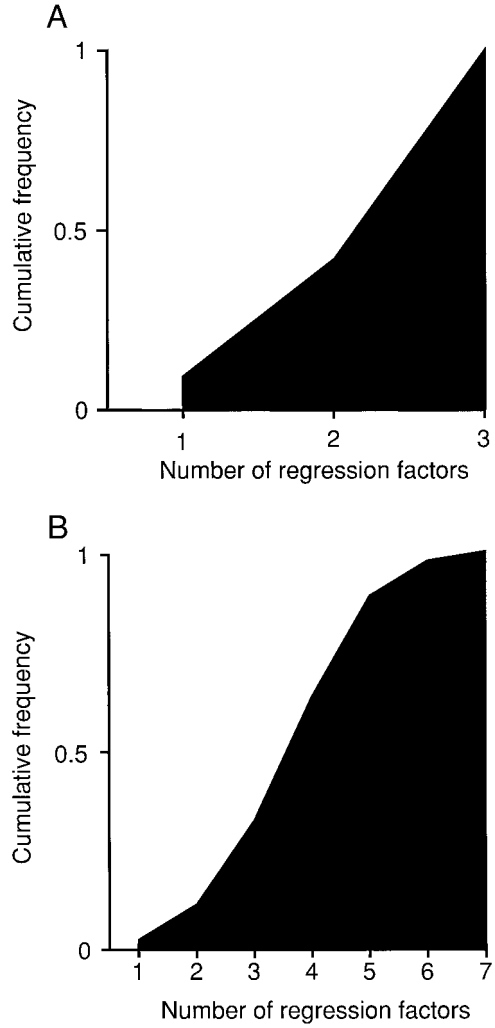

FIG. 11. Cumulative frequencies of the number of coordinates needed in each model to best fit each cortical unit's discharge rate. The hand velocity model (*A*) required all 3 coordinates to fit more than 50% of the discharge rate. In the JAV model (*B*), approximately 64% of the cortical unit discharge rates could be best fit by 4 or fewer joint angles.

ered to form a preferred direction in seven-dimensional space. These preferred directions represented unit vectors. The preferred directions were summed vectorially, and the resultant vector was calculated by dividing the sum by the number of

TABLE 4. *Comparison of raw versus square-root transformed data*

Regression Parameter	Raw Discharge Rates	Square-Root Transformed Discharge Rates
Anterior/posterior	55.0	51.5
Superior/inferior	20.4	23.5
Right/left	24.6	25.0
Shoulder adduction/abduction	8.6	10.4
Shoulder internal/external rotation	15.6	14.6
Shoulder flexion/extension	36.6	37.5
Elbow flexion/extension	25.8	24.5
Pronation/supination	2.7	3.1
Wrist flexion/extension	2.2	2.1
Wrist abduction/adduction	8.6	7.3

Values are percentages. The percentages indicate the frequency at which the parameter contributed most to the fit of the regression equation. The transformation has little effect on the results.

unit vectors. In the ideal case, the resultant vector from a uniform distribution would be exactly 0. We compared the resultant vector to a bootstrapped distribution of 1,000 resultant vectors randomly created from a uniform seven-dimensional distribution of unit vectors. A resultant vector of 0.0828 was found to be >95% of the bootstrapped distribution for the seven-dimensional space, while a smaller resultant could be considered representative of a uniform space. The magnitude of the JAV resultant used in this analysis was 0.0901 and is slightly above this criterion. The same analysis applied to a three-dimensional space (spherical distribution) gives a resultant vector of 0.0940 for the 95% confidence interval. The hand velocity resultant was >99% of the bootstrapped distribution (resultant vector = 0.2225). Although preferred directions from both models were not strictly uniform, the population vector gave accurate predictions of the hand's trajectory.

DISCUSSION

The "excess degrees of freedom" problem is a common theme in contemporary discussions of reaching (Haggard et al. 1995; Helms-Tillery et al. 1995; Sanger 2000). When moving through free space, only three of the seven DOF in the arm are needed to specify the position of the hand in space. This implies that to complete a reaching movement, the combination of joints used to rotate the arm segments must somehow be chosen from an infinite set of possibilities. Several studies have asked whether arm posture (specified by the combined set of joint angles) or hand displacement is represented in cortical activity (Caminiti et al. 1990; Kakei et al. 1999; Scott and Kalaska 1995, 1997). Although arm posture may have an effect on motor cortical activity, we have found single-cell and population activity to be more robustly related to hand velocity (Moran and Schwartz 1999b; Schwartz et al. 1988). Clearly the hand's trajectory is important behaviorally, as many studies have shown stereotypical reaching trajectories with invariant characteristics preserved across a wide set of conditions (Atkeson and Hollerbach 1985; Georgopoulos et al. 1981; Morasso 1981; Soechting et al. 1981).

Our previous work has demonstrated that the hand's velocity, that is, its speed and direction, is well represented in motor cortical activity during both reaching and drawing (Moran and Schwartz 1999a,b; Schwartz 1993; Schwartz and Moran 1999). For arm movements along the same path but in opposite directions, the motor cortical activity was differentially modulated, although the joint angles were the same for each point along the opposing paths (Moran and Schwartz 1999b). This

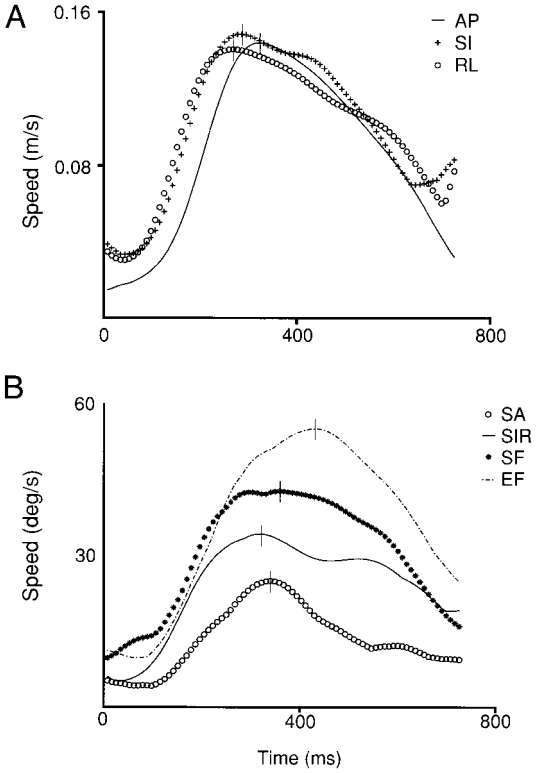

FIG. 12. Population vector predictions for (*A*) the 3 hand velocities and (*B*) the 4 dominant joint angular velocities (shoulder abduction/adduction, shoulder internal/external rotation, shoulder flexion/extension, and elbow flexion/extension). The relative peaks for the predicted hand velocities are consistent with those of the actual hand velocity. However, the predicted peak for shoulder flexion occurs more than 70 ms earlier than the predicted peak for elbow flexion even though the peaks overlap in the actual reach (compare with Fig. 3).

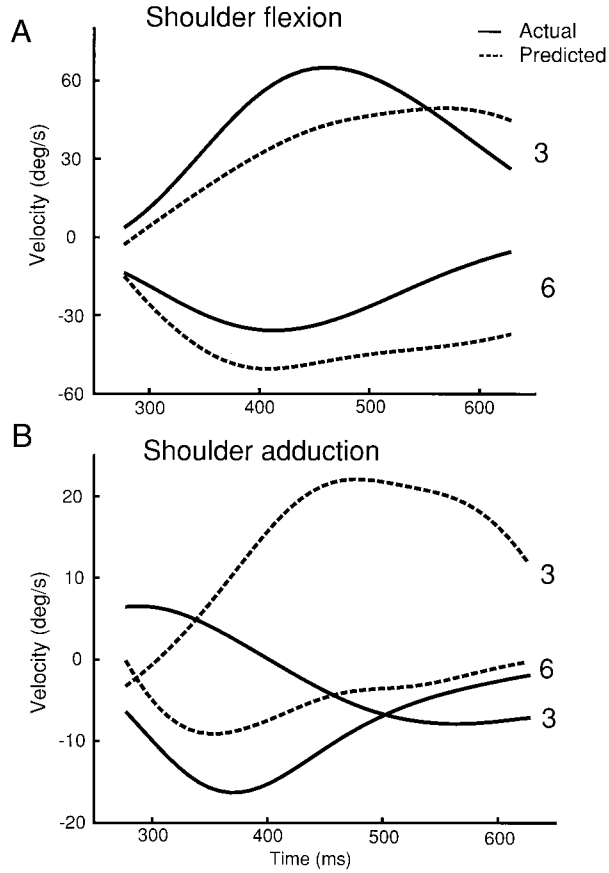

FIG. 13. Population vector predictions for the angular velocities of (*A*) shoulder flexion/extension and (*B*) shoulder adduction/abduction. The solid lines are the actual, measured angular velocities to *targets 3* and *6*. The dashed lines are the angular velocities predicted by the population vector model using the 7-DOF regression model. Note that the population vector model poorly predicts shoulder adduction to *target 3* but predicts shoulder flexion fairly well. Overall the population vector model predicted shoulder flexion/extension, elbow flexion/extension, and shoulder internal/external rotation to all targets better than the other joint angular velocities in the model. Further, the population vector prediction does not seem to match the prediction from the Jacobian analysis (compare with Fig. 5).

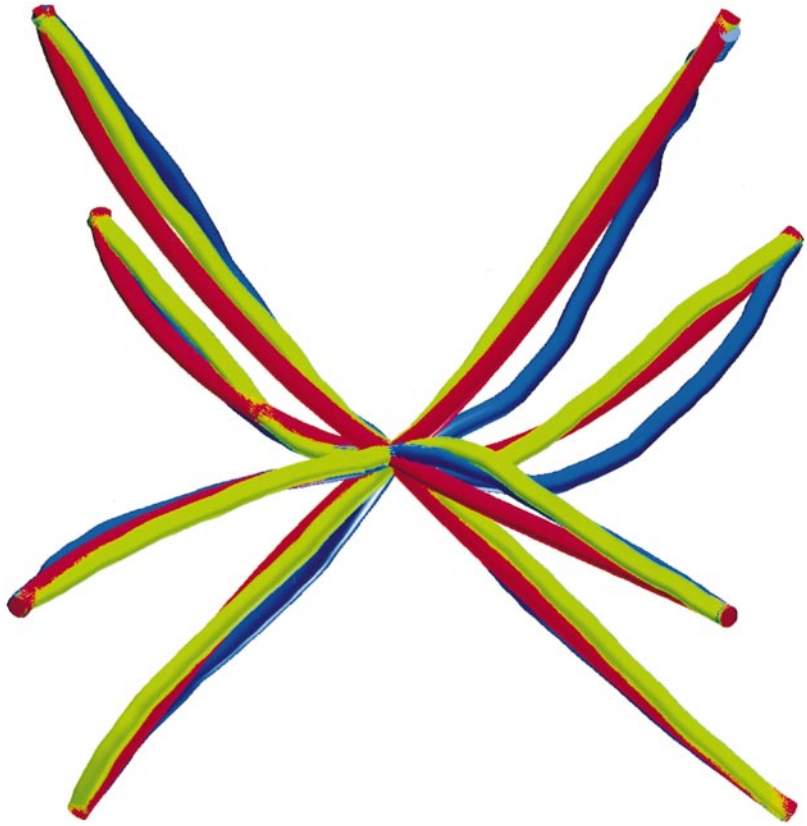

FIG. 14. Population vector trajectories for the hand during the center→out task created with the hand velocity tuning model (green) and the JAV tuning model (blue). The hand velocity model used 3 regression coefficients. The JAV model used 7 regression coefficients. The average, actual trajectory of the hand is shown in red. While qualitatively the JAV model population vector appears to have more error than the hand velocity model population vector, no clear difference in their root-mean-squared errors can be concluded when considering the inherent 4.5-mm error of the arm model.

implied that the joint angles per se were not well-correlated to cortical activity. However, if hand velocity is the extrinsic parameter represented in the population of cortical discharge rates, then joint angular velocity might be the more appropriate intrinsic parameter with which to make comparisons.

Recent studies have attempted to determine whether the selection of joint angles specifies the arm trajectory or is secondary to it (Caminiti et al. 1990; Kakei et al. 1999; Scott and Kalaska 1995, 1997). The overall conclusion of these studies has been that both intrinsic and extrinsic parameters can be correlated to the activity of individual cortical neurons. Indeed, our results confirm these past studies. However, our findings, both through direct correlation and the Jacobian matrix approach, suggest that hand velocity is well correlated to some joint angular velocities of the arm (specifically, shoulder flexion/extension, shoulder internal/external rotation, and elbow flexion/extension). In addition, the temporal relationship between the population of cortical units and joint angular velocity shows large errors in the predicted peaks of elbow and shoulder speeds (Fig. 12). Specifically, the shoulder flexion/extension preceded the elbow flexion/extension by over 70 ms even though the two peaked simultaneously during the actual reach. This corresponds to the results of Murphy et al. (1982), who found that the activity of "shoulder-related units" preceded that of "elbow-related units" in the reaching task. Although these timing discrepancies did not generate large errors in the handpath during reaching, this type of temporal offset could lead to significant handpath distortion in more complex tasks, such as drawing.

In summary, this study resulted in three findings: *1*) hand velocity and joint angular velocities were equally powerful predictors of motor cortical discharge rate; *2*) the subset of joint angular velocities required to predict neuronal activity in M1 adequately were well correlated to the extrinsic parameters; *3*) observations of joint angular "control" by M1 neurons may be a secondary to the high correlation between intrinsic and extrinsic reference frames.

Velocity-discharge correspondence

Moran and Schwartz (1999a) showed that the temporal profile of cortical discharge was well correlated to the bell-shaped velocity profile of the arm during reaching in a task that was similar to this. Therefore it is expected that any pair of bell-shaped profiles such as those generally found for the DOF in this experiment and hand velocity would be correlated. Nonetheless, it is interesting that velocity as a parameter is so well represented in the activity of these neurons. Behavioral studies (Soechting and Lacquaniti 1981) have shown that the velocity profile of the hand is bell-shaped, consistent in a wide range of reaching tasks, and the root of invariants such as isochrony and motor equivalence. This shape is ideal for both scaling and smoothness, criteria that make complex systems more efficient to control (Hollerbach and Flash 1982; Morasso et al. 1981).

Relative importance of angular degrees of freedom

JAVs of the shoulder and elbow tended to contribute more to the fit of the regression than those of the forearm and wrist. Wrist flexion and pronation contributed the least to the fit of the JAV model based on their standard, partial regression coefficients. Four possible explanations for this finding were considered: *1*) angular velocities for wrist flexion and pronation

varied little throughout the task (i.e., relatively constant joint angles); *2*) the sampled area of M1 contained few units that correlated with wrist and forearm movement; *3*) wrist flexion and pronation contributed little to the accurate performance of the reaching task; and *4*) relative importance of the joint angle may vary throughout the movement.

If the angular velocity for a particular joint had a low variance throughout the reach, its coefficient would generally not contribute much to the regression fit. Elbow flexion, shoulder flexion, and shoulder internal rotation are the joint angles that obtain the largest variations in speed during the center→out task (Fig. 3). This may have contributed to their relative importance in the regression. However, the joint angular speed for pronation was greater on average than that of shoulder adduction. Further, total angular displacement for pronation was also greater than that for shoulder adduction. Nevertheless, shoulder adduction had the largest standardized coefficient in 10.4% of the regressions, whereas pronation had the largest standardized coefficient in only 3.1% of the regressions. These data indicate that the importance of a particular joint velocity in the regression is not necessarily correlated with its variation within the movement.

The second possibility considered was that the sampled area of M1 contained few units that were correlated with wrist activity. After each unit was recorded, a passive examination of arm movement about each joint was performed. Of the 298 units studied, 253 had unequivocal modulations of activity about at least one joint. One hundred ninety-nine of the 253 (78.7%) were related only to passive movement of the shoulder and/or elbow. Only 54 of the 253 (21.3%) were related to passive movement of the wrist and/or hand. Thirty-two of the 54 wrist-related units were task related and had significant regression fits to joint angular velocity. The results of this wrist-related subpopulation of cortical units were similar to those of the entire population: namely, the best regression typically required four or less joint angular velocities, and the shoulder and elbow angular velocities contributed most to the fit of the regression. It is unlikely therefore that the sampled area of M1 biased the results.

If movement about a particular joint (e.g., wrist flexion) did not contribute substantially to the accuracy of the reaching task, then that movement may have contributed less to the fit of the regression. In the experimental setup, the IRED marker that controlled the cursor was positioned on the hand dorsum. It is likely that wrist movements generated only relatively small displacements of the cursor toward the target in comparison to movements of the shoulder and elbow. This was tested by selectively removing different joint rotations from the kinematic arm model and measuring the resulting errors in reach. The models without shoulder flexion, elbow flexion, and shoulder internal rotation had RMS errors of 24.4, 32.8, and 29.4 mm. The error produced by these models is more than five times that of the full model (full model = 4.5 mm). Without the remaining joint angles, the models also had statistically significant increases in error: shoulder adduction (mean 6.5 mm), pronation (7.1 mm), wrist flexion (5.3 mm), and wrist abduction (5.0 mm). However, these errors were much smaller than those of shoulder internal rotation, shoulder flexion, and elbow flexion (only 1.1–1.6 times the error of the full model). Wrist flexion and pronation make statistically significant, yet relatively small contributions to hand displacement in this reaching task.

The fourth possibility we considered was that the relative importance of the joint angular velocities varied throughout the task. We re-analyzed the reaching movement using the discharge rates within the reaction time (RT, epoch from the target's appearance to the onset of movement) and the movement time (MT, epoch from the movement onset to offset). The relative importance of the joint angular velocities and the number of regressors for the best model were equivalent across epochs.

Extrinsic versus intrinsic space

The transformation from hand position to joint posture is both nonunique and nonlinear. For a reasonably small workspace, with only two DOF, and assuming stereotypical movements, the inverse of the Jacobian matrix ($J[p, \theta]^{+}$) has been theorized to describe a locally linear relationship between hand velocity and joint angular velocity (Mussa-Ivaldi 1988). Indeed, our data were so consistent for three of the arm angles, both within a single movement and between movements to different targets, that we were able to use a simple linear regression to perform inverse kinematics on the joint angular velocities (Table 3). These same angles were also well predicted in the Jacobian analysis.

However, the remaining four joint angular velocities were not as well correlated with extrinsic coordinates. We estimated joint angular velocities from the actual hand velocities using either a Jacobian matrix that was calculated at the center position in the workspace and held constant, or a Jacobian matrix that was re-calculated at each instantaneous posture (i.e., bin) during the reach. Table 5 shows the RMS error for each estimated joint angular velocity as a percentage of the actual, mean joint angular velocity. The Jacobian approach clearly failed to predict shoulder adduction/abduction or the distal three DOF, and this approach is unsuitable for predicting these four DOF. Further, it has been assumed for reasonably

TABLE 5. *RMS error as a percentage of the actual, mean joint angular velocity*

	%RMS Error	
Joint Angular Velocity	Constant Jacobian Matrix	Continuously Recalculated Jacobian Matrix
Shoulder adduction/abduction	28.1	29.3
Shoulder internal/external rotation	6.3	5.2
Shoulder flexion/extension	17.6	4.4
Elbow flexion/extension	21.7	4.3
Pronation/Supination	13.7	13.4
Wrist flexion/extension	16.2	18.9
Wrist abduction/adduction	11.6	12.0

The joint angular velocity was estimated at each movement bin from the hand velocity by the Jacobian using 2 methods. In the 1st method (1st column), a Jacobian matrix was calculated at the beginning of the movement (hand in the center of the workspace) and held constant throughout the reach. In the 2nd method (2nd column), the Jacobian matrix was recalculated at every bin during the reach. The RMS error was calculated between the estimated and actual angular velocities. It was then made into a percentage of the actual, mean joint angular velocity, a value found by calculating the sum of the squares for the 7 angular velocities and determining the mean of this value over all bins in the movement. RMS, root-mean-squared.

small workspaces that the Jacobian matrix would be relatively constant. However, the RMS error for shoulder and elbow flexion/extension is much lower for the continuously calculated estimate than for the constant estimate (Table 5), showing that the assumption of a constant Jacobian matrix does not give optimal results.

A fair number of recorded units (44%) were driven by passive adduction/abduction of the shoulder, which shows that the topographical region of motor cortex we sampled contained units sensitive to this type of angular displacement. However, the Jacobian method and the population vector method generally made different predictions of this parameter, and neither prediction was very accurate. This suggests that the good prediction of the other three joint angular velocities by the population vector analysis is due to their strong correlation with the extrinsic velocity of the hand. This population analysis was able to detect changes in timing between those three joint angles that neither the Jacobian nor the correlation could detect. Both results lead us to conclude that extrinsic parameters are better represented than intrinsic parameters in the cortical activity. However, more experiments using tasks where the two reference frames are more dissociated will be needed to substantiate this conclusion.

Nonetheless, it is useful to emphasize the strong correlation between three of the main intrinsic DOFs and the extrinsic hand velocity. This correlation during such a common, natural movement such as unconstrained reaching may be indicative of an optimized planning strategy. Such a characteristic would have the advantage of obviating an explicit step or calculation between reference frames.

This work was supported by the McDonnell-Pew Foundation and the Neurosciences Research Foundation.

REFERENCES

ASANUMA H AND ROSEN I. Topographical organization of cortical efferent zones projecting to distal forelimb muscles in the monkey. *Exp Brain Res* 14: 243–256, 1972.

ASHE J AND GEORGOPOULOS AP. Movement parameters and neural activity in motor cortex and area 5. *Cereb Cortex* 4: 590–600, 1994.

ATKESON CG AND HOLLERBACH JM. Kinematic features of unrestrained vertical arm movements. *J Neurosci* 5: 2318–2330, 1985.

BERNSTEIN NA. *The Coordination and Regulation of Movements.* Oxford, UK: Pergamon, 1967.

CAMINITI R, JOHNSON PB, AND URBANO A. Making arm movements within different parts of space: dynamic aspects in the primate motor cortex. *J Neurosci* 10: 2039–2058, 1990.

CARPENTER AF, GEORGOPOULOS AP, AND PELLIZZER G. Motor cortical encoding of serial order in a context-recall task. *Science* 283: 1752–1757, 1999.

EVARTS EV. Relation of pyramidal tract activity to force exerted during voluntary movement. *J Neurophysiol* 31: 14–27, 1968.

FLANDERS M, TILLERY SI, AND SOECHTING JF. Early stages in a sensorimotor transformation. *Behav Brain Sci* 15: 309–362, 1992.

FURNIVAL GM AND WILSON RW. Regressions by leaps and bounds. *Technometrics* 16: 499–511, 1974.

GEORGOPOULOS AP, ASHE J, SMYRNIS N, AND TAIRA M. The motor cortex and the coding of force. *Science* 256: 1692–1695, 1992.

GEORGOPOULOS AP, KALASKA JF, CAMINITI R, AND MASSEY JT. On the relations between the direction of two-dimensional arm movements and cell discharge in primate motor cortex. *J Neurosci* 2: 1527–1537, 1982.

GEORGOPOULOS AP, KALASKA JF, AND MASSEY JT. Spatial trajectories and reaction times of aimed movements: effects of practice, uncertainty, and change in target location. *J Neurophysiol* 46: 725–743, 1981.

GEORGOPOULOS AP, LURITO JT, PETRIDES M, SCHWARTZ AB, AND MASSEY JT. Mental rotation of the neuronal population vector. *Science* 243: 234–236, 1989.

HAGGARD P, HUTCHINSON K, AND STEIN J. Patterns of coordinated multi-joint movement. *Exp Brain Res* 107: 254–266, 1995.

HELMS-TILLERY SI, EBNER TJ, AND SOECHTING JF. Task dependence of primate arm postures. *Exp Brain Res* 104: 1–11, 1995.

HOLLERBACH JM AND FLASH T. Dynamic interactions between limb segments during planar arm movement. *Biol Cybern* 44: 67–77, 1982.

HUMPHREY DR. Representation of movements and muscles within the primate precentral motor cortex: historical and current perspectives. *Federation Proc* 45: 2687–2699, 1986.

HUMPHREY DR, SCHMIDT EM, AND THOMPSON WD. Predicting measures of motor performance from multiple cortical spike trains. *Science* 170: 758–762, 1970.

JACKSON JH. On the comparative study of diseases in the nervous system. *Br Med J* 2: 355–362, 1889.

KAKEI S, HOFFMAN DS, AND STRICK PL. Muscle and movement representations in the primary motor cortex. *Science* 285: 2136–2139, 1999.

KALASKA JF AND CRAMMOND DJ. Cerebral cortical mechanisms of reaching movements. *Science* 255: 1517–1523, 1992.

MARTINO AM AND STRICK PL. Corticospinal projections originate from the arcuate premotor area. *Brain Res* 404: 307–312, 1987.

MORAN DW AND SCHWARTZ AB. Motor cortical activity during drawing movements: population representation during spiral tracing. *J Neurophysiol* 82: 2693–2704, 1999a.

MORAN DW AND SCHWARTZ AB. Motor cortical representation of speed and direction during reaching. *J Neurophysiol* 82: 2676–2692, 1999b.

MORASSO P. Spatial control of arm movements. *Exp Brain Res* 42: 223–227, 1981.

MOUNTCASTLE VB, LYNCH JC, GEORGOPOULOS A, SAKATA H, AND ACUNA C. Posterior parietal association cortex of the monkey: command functions for operations within extrapersonal space. *J Neurophysiol* 38: 871–908, 1975.

MOUNTCASTLE VB, TALBOT WH, SAKATA H, AND HYVARINEN J. Cortical neuronal mechanisms in flutter-vibration studied in unanesthetized monkeys. Neuronal periodicity and frequency discrimination. *J Neurophysiol* 32: 452–484, 1969.

MURPHY JT, KWAN HC, MACKAY WA, AND WONG YC. Precentral unit activity correlated with angular components of a compound arm movement. *Brain Res* 246: 141–145, 1982.

MUSSA-IVALDI FA. Do neurons in the motor cortex encode movement direction? An alternative hypothesis. *Neurosci Lett* 91: 106–111, 1988.

RICHMOND BJ, OPTICAN LM, PODELL M, AND SPITZER H. Temporal encoding of two-dimensional patterns by single units in primate inferior temporal cortex. I. Response characteristics. *J Neurophysiol* 57: 132–146, 1987.

SANGER TD. Human arm movements described by a low-dimensional superposition of principal components. *J Neurosci* 20: 1066–1072, 2000.

SCHMIDT EM, JOST RG, AND DAVIS KK. Reexamination of the force relationship of cortical cell discharge patterns with conditioned wrist movements. *Brain Res* 83: 213–223, 1975.

SCHWARTZ AB. Motor cortical activity during drawing movements: single-unit activity during sinusoid tracing. *J Neurophysiol* 68: 528–541, 1992.

SCHWARTZ AB. Motor cortical activity during drawing movements: population representation during sinusoid tracing. *J Neurophysiol* 70: 28–36, 1993.

SCHWARTZ AB, KETTNER RE, AND GEORGOPOULOS AP. Primate motor cortex and free arm movements to visual targets in three-dimensional space. I. Relations between single cell discharge and direction of movement. *J Neurosci* 8: 2913–2927, 1988.

SCHWARTZ AB AND MORAN DW. Motor cortical activity during drawing movements: population representation during lemniscate tracing. *J Neurophysiol* 82: 2705–2718, 1999.

SCOTT SH AND KALASKA JF. Changes in motor cortex activity during reaching movements with similar hand paths but different arm postures [published errata appear in *J Neurophysiol* 1997 Jan:77(1): following table of contents and 1997 Jun:77(6): 2856]. *J Neurophysiol* 73: 2563–2567, 1995.

SCOTT SH AND KALASKA JF. Reaching movements with similar hand paths but different arm orientations. I. Activity of individual cells in motor cortex. *J Neurophysiol* 77: 826–852, 1997.

SOECHTING JF AND LACQUANITI F. Invariant characteristics of a pointing movement in man. *J Neurosci* 1: 710–720, 1981.

SOECHTING JF AND FLANDERS M. Errors in pointing are due to approximations in sensorimotor transformations. *J Neurophysiol* 62: 595–608, 1989.

SOKAL RR AND ROHLF FJ. *Biometry*. New York: Freeman, 1997.

TODOROV E. Direct cortical control of muscle activation in voluntary arm movements: a model. *Nat Neurosci* 3: 391–398, 2000.

WOLTRING HJ. A Fortran package for generalized, cross-validatory spline smoothing and differentiation. *Adv Eng Software* 8: 104–113, 1986.